Multi-colour power splitters based on femtosecond-laser-written directional couplers

Author: **MATTEO BALEN**

Advisor: **PROF. ROBERTO OSELLAME**

Co-advisor: **DR. FRANCESCA BRAGHERI**

Academic year: **2021-2022**

1. Introduction

In recent years the field of optical microscopy was characterized by raising interest in the realization of integrated optical systems defined as Microscopes on Chip (MOCs). These devices are aimed at the miniaturization and integration of advanced optical and microfluidic systems in a single compact chip. This integration could revolutionize the use of optical microscopes, offering the possibility to realize high-quality imaging without the need for expensive and hard-to-manage bulk optics. The main components of a MOC are an integrated optical circuit for delivering light and microfluidic channels for transporting and manipulating the samples [1]. A noteworthy technique that is particularly apt for the realization of such devices is Femtosecond Laser Micromachining (FLM). This technique in fact allows the realization of both fluidic and optical components integrated on the same chip [2]. Furthermore, the outstanding capability of FLM to realize almost arbitrary 3-dimensional structures makes it particularly interesting for the realization of MOCs, which may require complex systems to be realized. Among the different techniques of optical microscopy, Light-Sheet Fluorescence Microscopy (LSFM) is exceptionally well-suited for its integration in a

MOC. LSFM consists of the illumination of samples, stained with fluorescent markers, with a thin sheet of light, which optically sections the sample exciting its fluorescence selectively slice by slice. The images pertaining to multiple slices of the specimen are then stacked one on top of the other and a 3-dimensional reconstruction of the sample is achieved [3]. Typically, in a MOC the samples are transported to the imaging region by suspending them in a solution and flowing them through microchannels. This way of transportation is especially beneficial for LSFM which already requires the scanning of the sample through the light-sheet. Besides the optical sectioning property, this microscopy technique possesses several advantages that make it particularly interesting for the imaging of biological samples: the fast acquisition time granted by the wide-field collection of the fluorescence signal and the selective illumination which grants low photo-toxicity and absence of background noise [4]. LSFM is characterised by a lateral resolution that is limited by diffraction, thus it cannot be employed for the imaging of subcellular structures. However, this technique can be integrated with Structured Illumination Microscopy (SIM), which can be exploited to attain super-resolution. In SIM the samples are illumi-

nated with light that presents a spatial modulation. This modulation enriches the information content of the retrieved image and allows to obtain a resolution that surpasses the diffraction limit [5]. The most common method of creating a patterned illumination is by the interference of mutually coherent laser beams. The integration of these two techniques can be addressed as light-sheet SIM, its simplest implementation is achieved by creating multiple light-sheets that are made to interfere on the sample. This way, the patterned light-sheet arising from the interference of the fields, grants simultaneously optical sectioning and a modulated illumination in the plane that allows attaining super-resolution.

This thesis work has been carried out within a project aimed at the realization of a light-sheet structured illumination microscope on-chip, with the fabrication techniques of FLM. In particular, the focus of the activity was on the realization of an integrated optic circuit for the delivery of laser light to the illumination section of the chip. The MOC under design is characterized by a three-way illumination with interfering light-sheets, therefore it was necessary to realize a light delivery circuit, denominated as *tritter*, that would take an input laser beam and divide its power equally on the three distinct light-sheets [6]. One of the relevant features of a fluorescence microscope is the capability to selectively and contemporarily excite different fluorophores. In fact, distinct markers can be utilized to identify specific structures in the sample under study. For this reason, the objective of this thesis work was to realize an integrated optical circuit insensitive to the illumination wavelength. The chosen design for the realization of the device is schematized in figure 1. To achieve the desired splitting ratio two directional couplers are cascaded one after the other. The power injected in the input waveguide firstly is split among two waveguides with ratio ⅔–⅓, then the second coupler splits the ⅔ equally on the third waveguide, yielding a uniform power splitting at the output of the tritter.

2.   Waveguides and Couplers

The first step towards the realization of a multi-wavelength tritter is the identification of a set of fabrication parameters allowing for the realization of high-quality single-mode optical waveg-
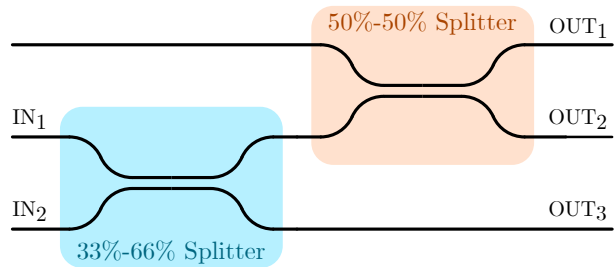

Figure 1: Schematic representation of a tritter.

uides. The waveguides studied in this work were realized by irradiating chips of alumino-borosilicate glass — sold by Corning® under the commercial name of Eagle XG — with ∼300 fs laser pulses from a cavity-dumped Yb:KYW oscillator at 1030 nm with repetition rate of 1 MHz. The laser pulses were focused on the chip with a 50× magnification objective 0.65 NA with correction collar (Olympus). To study the waveguides losses, laser light at visible wavelengths was fibre butt-coupled to the fabricated waveguides. The losses investigated are the coupling losses (CL), determined by the overlap of the modes of the injection fibre and the waveguide, the propagation losses (PL), related to the absorption and/or scattering of light along the waveguide, and the bending losses (BL), arising from the radiation of power outside of the waveguide in the presence of curvature. Mainly two fabrication parameters have been investigated in the performance optimization, namely the power of the irradiation and the inscription velocity. A good set of fabrication parameters was identified which yielded low-losses waveguides, reported in table 1, and single-mode operation at all the wavelengths investigated. These results pertain to waveguides realized at the depth of 15 μm with an irradiation power of 230 mW. Each waveguide was scanned 8 times at the velocity of 40 mm/s in the same direction. The radius of curvature for the estimation of the bending losses is equal to 30 mm. The same parameters

λ [nm]	PL $\left[\frac{dB}{cm}\right]$	BL $\left[\frac{dB}{cm}\right]$	CL [dB]
488	0.311	0.335	0.132
532	0.186	0.359	0.038
561	0.325	0.279	0.038
635	0.212	2.039	0.128

Table 1: Average waveguide losses measured.
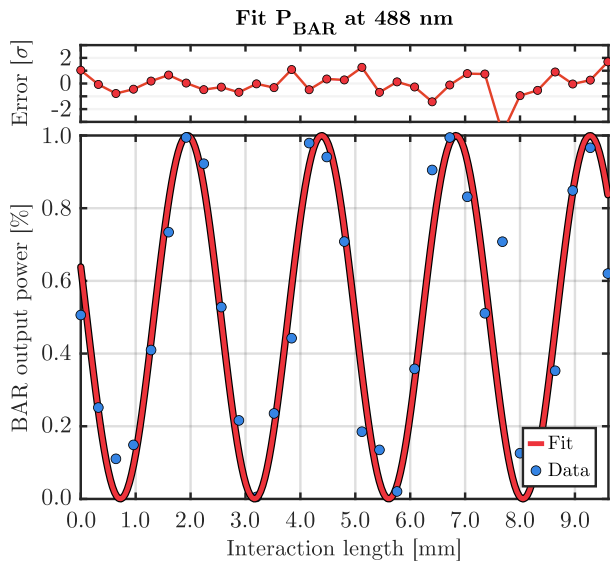
Fit P$_{\text{BAR}}$ at 488 nm

Figure 2: Bar output power measured at 488 nm of a set of couplers with $d = 4.0\,\mu$m and L from 0 to 9.6 mm with step 0.320 mm.

were used to fabricate sets of directional couplers. A directional coupler (DC) consists of two waveguides that are brought close to each other at a distance d, defined interaction distance, for a length L, defined interaction length. In the interaction region, the two distinct waveguides are close enough that the tails of the optical guided modes overlap and power exchange occurs. This exchange of power can be studied recurring to coupled mode theory (CMT) [7]. According to this theory, the power P_{BAR} measured at its output and the power P_{CROSS} coupled in the adjacent waveguide can be described by the following:

$$\begin{cases} P_{BAR} & = \cos^2\left(kL + \varphi_0\right) \\ P_{CROSS} & = \sin^2\left(kL + \varphi_0\right) \end{cases}$$

where the coupling coefficient k governs the rate of the oscillatory power exchange between the waveguides, while φ_0 is a spurious component related to the coupling occurring in the curved region of the coupler. The division of power at the two outputs of the directional coupler can be tuned to match a required value if all the parameters are known and controllable. The coupling coefficient is described by a complex dependence on the characteristics of the two waveguides, yet it possesses a straightforward dependence on the interaction distance. In fact, an exponential dependence of the type $k = a \exp\left(-b \cdot d\right)$, can be identified. Two distinct kinds of data-fitting procedures have been realized to estimate the coupling coefficient of the DCs realized with FLM

by varying the two parameters L and d. In the first case, batches of couplers have been realized by fixing all the parameters and varying the interaction length in an ample range. This procedure allowed the verification of the sinusoidal dependence of the output power of the couplers realized experimentally, as well as the estimation of the value of k at a given interaction distance, as exemplified in figure 2 for the case of $d = 4.0\,\mu$m and L from 0 to 9.6 mm with step 0.320 mm measured at 488 nm.
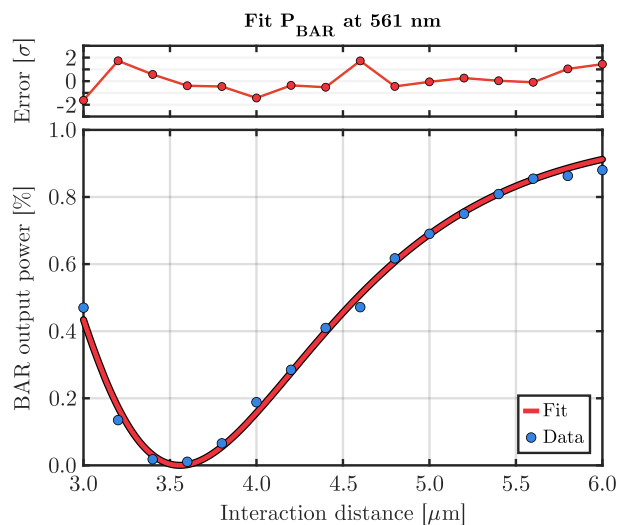
Fit P$_{\text{BAR}}$ at 561 nm

Figure 3: Bar output power measured at 561 nm of a set of couplers with $L = 0$ and d variable from 3.0 to 6.0 μm with step 0.2 μm.

The second approach consists in measuring sets of couplers fabricated with variable interaction distance, while all the other parameters are kept fixed. The results measured at 561 nm regarding the case of $L = 0$ and d variable from 3.0 to 6.0 μm with step 0.2 μm are represented in figure 3. This procedure allowed to estimate the dependence of k on the interaction distance. Both the results obtained were in accordance with the ones expected from CMT. It was thus possible to characterise the dependence of the coupling coefficient on the interaction distance at all the wavelengths analysed (488, 532, 561, 607 and 635 nm). From these data, it was possible to realize directional with a desired splitting ratio at single wavelengths. The dependence of the coupling coefficient with the wavelength was then analysed and a positive linear relationship was highlighted between k and λ, as expected from theoretical considerations. Unfortunately, this strong wavelength dependence, highlighted
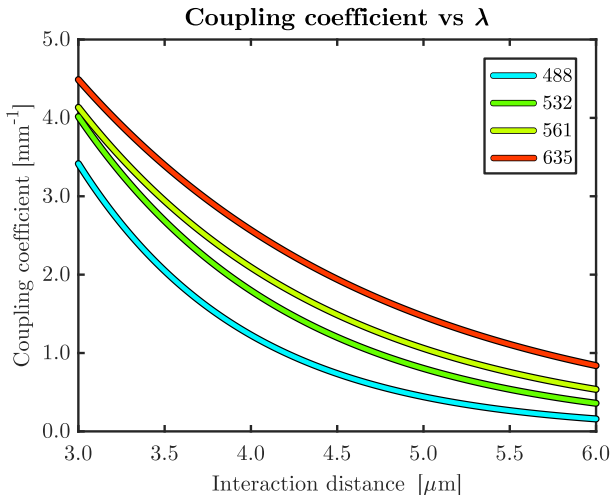
Figure 4: Exponential dependence of k at the wavelengths 488, 532, 561 and 635 nm.

in figure 4, does not allow the straightforward realization of power splitters suitable for operation at multiple wavelengths. Two distinct approaches have been devised to overcome this limitation and are detailed in the following sections.

3. Dual and tri-colour tritter

The first approach followed in the realization of multi-wavelength power splitters is discussed in this section. Specifically, it has been identified a method for the realization of couplers showing the desired splitting ratio at distinct wavelengths, selected by design. It was verified that to distinct wavelengths corresponds a different coupling coefficient, thus the power exchange among the waveguides is characterized by a sinusoid with different period according to the wavelength injected. Since the couplers have a periodic dependence on the output power with respect to the length of the interaction regions, two distinct wavelengths can share the exact splitting ratio at appropriately selected values of L. As an example, figure 5 reports the case of a dual-colour coupler targeted at 488
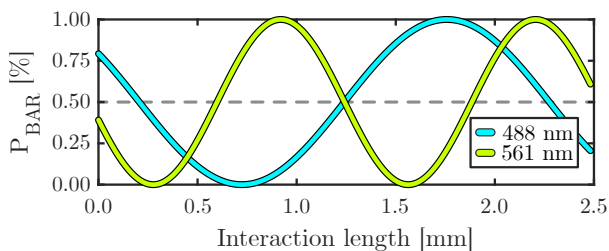

Figure 5: Simulated response of dual-colour coupler with $d = 3.95\,\mu\text{m}$ at 488 and 561 nm.

Algorithm 1 Multi-colour coupler finder

1: Define target splitting ratio T
2: **for** d *in range* **do**
3:     Calculate k and φ_0 at λ_j
4:     **for** L *in range* **do**
5:         Compute $BAR(k, L, \varphi_0)$ power at λ_j
6:         Calculate $\varepsilon = \sum_{\lambda_j} |BAR - T|$
7:         **if** ε *is the smallest* **then**
8:             Save current geometry $[d, L]$
9:         **end if**
10:     **end for**
11: **end for**
12: Return best geometry found

and 561 nm with splitting ratio of 50%. Furthermore, controlling the coupling coefficient by tuning the interaction distance, two or more sinusoids — pertaining to distinct wavelengths — can be matched at the same output power. Algorithm 1 reports the numerical procedure devised to identify coupler geometries, d and L, that satisfy the requirement of identical splitting ratio at distinct wavelengths λ_j.

λ	488 nm	561 nm
$P_{out,1}$	38.9 %	32.8 %
$P_{out,2}$	33.8 %	35.8 %
$P_{out,3}$	27.4 %	31.4 %

Table 2: Measured splitting ratio of dual-colour tritter 488/561 nm.

This procedure was utilized for the identification of couplers with splitting ratios of $33.\bar{3}\%, 50\%$ and $66.\bar{6}\%$ and tested experimentally in two devices. The first device was designed for the wavelengths 488 and 561 nm, while the second device was targeted at the three wavelengths 488, 561, and 635 nm. Both resulted in satisfactory power splitting, reported in table 2 and 3 respectively, proving the correctness of this fabrication method. In fact, it was possible to realize a tritter with accurate power division at its output, at each wavelength, as designed. Furthermore, by evaluating the contrast expected by such power splitting, the results yield values of 99.57% and 98.45% respectively, which should lead to an optimal contrast of the modulation pattern realized for a structured illumination microscope.

λ	488 nm	561 nm	635 nm
$P_{out,1}$	29.1 %	26.2 %	46.1 %
$P_{out,2}$	41.7 %	35.5 %	27.8 %
$P_{out,3}$	29.1 %	38.3 %	26.1 %

Table 3: Measured splitting ratio of tri-colour tritter 488/561/635 nm.

4.   Broadband couplers

To obtain a broadband tritter with the design identified and illustrated previously, it is necessary to manufacture broadband couplers with the different splitting ratios required. To realize broadband couplers, capable of delivering a splitting ratio insensitive to the wavelengths, asynchronous couplers were utilized. A coupler that is composed of non-identical waveguides is defined as asynchronous and is characterised by a response that differs from the synchronous counterpart. According to CMT, the output power of these devices reads:

$$P_{BAR} = 1 - \frac{k^2}{k^2 + \frac{\Delta\beta^2}{4}} \sin^2\left(\sqrt{k^2 + \frac{\Delta\beta^2}{4}}L + \varphi_0\right)$$

where the detuning parameter $\Delta\beta \triangleq \beta_1 - \beta_2$ describes the difference of the propagation constant of the modes guided by the two waveguides. The presence of a detuning has the effect of diminishing the colour dispersion introduced by the strong dependence of the coupling coefficient with the wavelength. To realize couplers with non-identical waveguides several variations on the fabrication procedure were explored. The most effective technique identified consists of irradiating the two arms of the coupler at different translation velocities. This method provides the possibility to tune the amount of detuning by regulating the velocity difference Δv of the two arms. In fact, it has been highlighted a positive linear relationship between $\Delta\beta$ and the absolute velocity difference, as highlighted in figure 6. Furthermore, it was studied the dependence of the detuning obtained at each value of Δv as a function of the wavelength. This study identified a linear dependence of $\Delta\beta$ with the wavelength, which is not in agreement with the theory. In fact, a dependence of the type $1/\lambda$ was expected. Nonetheless, the experimental dependence identified was utilized for the realization of
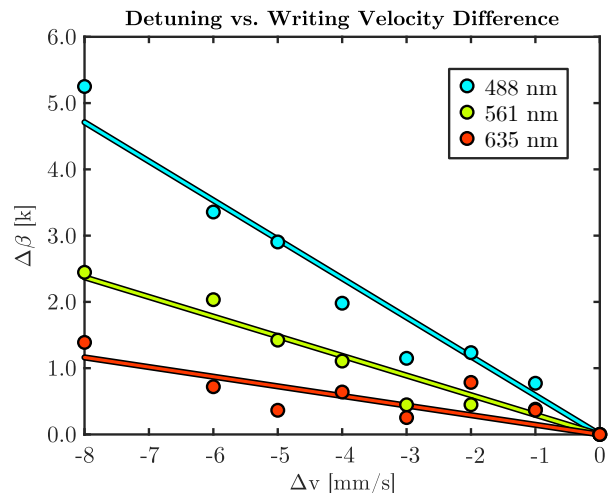

Figure 6: Detuning obtained with different values of Δv at 488, 561 and 635 nm.

broadband couplers with the methods described in the following. Algorithm 2 reports the numerical procedure utilized for the identification of the parameters, d, L and Δv suitable for the realization of broadband couplers. This algorithm aims at identifying solutions yielding the greatest extension of the bandwidth, intended as the range of frequencies at which the splitting ratio is within a specified distance from the target. With this method, it was possible to

---

Algorithm 2 Broadband coupler finder

1: Define target splitting ratio T
2: Indicate target wavelengths λ_j
3: Define tolerance from the target, err
4: **for** d in $range$ **do**
5:     Calculate k and φ_0 at λ_j
6:     **for** Δv in $range$ **do**
7:         Calculate $\Delta\beta$ $\forall\lambda$
8:         **for** L in $range$ **do**
9:             Compute $BAR(k, L, \varphi_0, \Delta\beta)$ $\forall\lambda$
10:             Calculate $\varepsilon = \sum_{\lambda_j} |BAR - T|$
11:             **for** λ in $range$ **do**
12:                 **if** $|BAR - T| < err$ **then**
13:                     Increment bandwidth BW
14:                 **end if**
15:             **end for**
16:             **if** ε/BW^α is the $smallest$ **then**
17:                 Save current parameters $[d, L, \Delta v]$
18:             **end if**
19:         **end for**
20:     **end for**
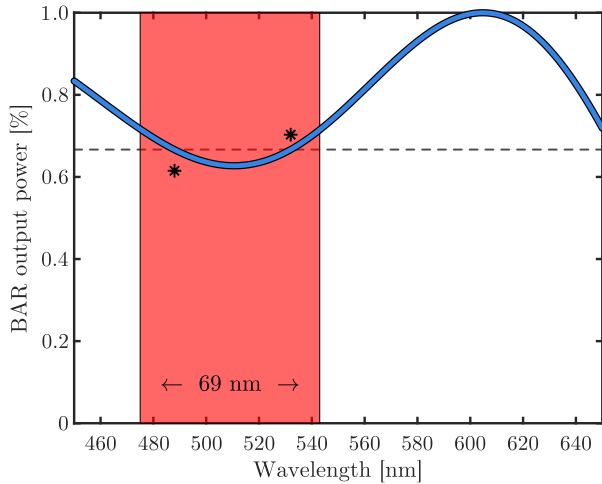21: **end for**
22: Return best fabrication parameters found

Figure 7: Simulated and measured response of broadband coupler with $d = 4.25$ μm, $L = 1.006$ mm and $\Delta v = -3.8$ mm/s.

simulate possible devices at the splitting ratio of $33.\bar{3}\%$, 50% and $66.\bar{6}\%$ with bandwidths as large as 100 nm. To validate this methodology multiple asynchronous couplers were fabricated with the parameters identified. Figure 7 reports the results obtained for one of the realized devices. The simulated response and expected bandwidth are reported in the blue line and red-shaded region. The expected bandwidth of 69 nm is centred between 488 and 532 nm at the splitting ratio of $66.\bar{6}\%$. Two different wavelengths have been experimentally measured to verify the simulations. The results, indicated by the black markers in the figure, show a good agreement between simulation and experiment thus representing solid evidence of the possibility to obtain broadband couplers with this methodology. Additional measurements, realized at multiple intermediate wavelengths are required to confirm the existence of a bandwidth around the desired splitting ratio and estimate its width. It is worth underlying that other tested devices with larger expected bandwidth and different splitting ratios showed a significant deviation from the simulated behaviour. Therefore we argue that further analysis of the impact of the detuning on the response of directional couplers is required.

5. Conclusions

In conclusion, the work presented reports on different solutions for the realization of multicolour power splitters, each with its own mer-

its and limits. The first method implemented dealt with the operation at selected wavelengths while the latter approach implemented a coupler with operation over an extended bandwidth. We can envisage the first approach to be particularly suitable for fluorescence microscopy applications in which the markers of interest are far from each other in the spectral range. This method proved to be successful but presents some issues as the limited number of operating wavelengths and their choice. Conversely, the second approach could be suitable for those applications in which tightly spaced wavelengths are selected in a narrower bandwidth. This method allows instead greater freedom in the selection of the spectral region of operation. Further experimentation is still required to quantify precisely which is the extent of the bandwidth of the splitters realized with such a method. Future analysis foresees deepening the understanding of the behaviour of asynchronous couplers at the short visible wavelengths as required by fluorescence imaging.

References

[1] P. Paiè et al. "Microfluidic based optical microscopes on chip". In: *Cytometry Part A* 93.10 (2018), pp. 987–996.

[2] R. Osellame et al. "Femtosecond laser microstructuring: an enabling tool for optofluidic lab-on-chips". In: *Laser & photonics reviews* 5.3 (2011), pp. 442–463.

[3] J. Huisken et al. "Optical sectioning deep inside live embryos by selective plane illumination microscopy". In: *Science* 305.5686 (2004), pp. 1007–1009.

[4] F. Sala et al. "High-throughput 3D imaging of single cells with light-sheet fluorescence microscopy on chip". In: *Biomedical optics express* 11.8 (2020), pp. 4397–4407.

[5] M. G. Gustafsson. "Surpassing the lateral resolution limit by a factor of two using structured illumination microscopy". In: *Journal of microscopy* 198.2 (2000), pp. 82–87.

[6] M. Calvarese et al. "Integrated optical device for Structured Illumination Microscopy". In: *Optics Express* 30.17 (2022), pp. 30246–30259.

[7] R. G. Hunsperger. *Integrated optics.* Vol. 4. Springer, 1995.